## The Q2 dependence of the structure function ratio F2Sn / F2C and the difference RSn-RC in deep inelastic muon scattering.

Arneodo, M.; Ballintijn, M.; Ketel, T.J.; van Middelkoop, G.

***published in***
Nuclear Physics B
1996

***DOI (link to publisher)***
10.1016/S0550-3213(96)00537-8

***document version***
Publisher's PDF, also known as Version of record

ELSEVIER

Nuclear Physics B 481 (1996) 23–39

NUCLEAR PHYSICS B

# The $Q^2$ dependence of the structure function ratio $F_2^{Sn}/F_2^C$ and the difference $R^{Sn} - R^C$ in deep inelastic muon scattering

The New Muon Collaboration (NMC)

M. Arneodo[ℓ,1], A. Arvidson[m], B. Badełek[m,o], M. Ballintijn[h], G. Baum[a], J. Beaufays[h], I.G. Bird[c,h,2], P. Björkholm[m], M. Botje[k,3], C. Broggini[g,4], W. Brückner[c], A. Brüll[b,5], W.J. Burger[k,6], J. Ciborowski[o], R. van Dantzig[h], H. Döbbeling[c], A. Dyring[m], H. Engelien[b], M.I. Ferrero[ℓ], L. Fluri[g], U. Gaul[c], T. Granier[i,7], M. Grosse-Perdekamp[b,8], D. von Harrach[c,9], M. van der Heijden[h], C. Heusch[j], Q. Ingram[k], M. de Jong[h,2], E.M. Kabuß[c,9], R. Kaiser[b], T.J. Ketel[h], F. Klein[e,10], S. Kullander[m], K. Kurek[o], U. Landgraf[b], T. Lindqvist[m], G.K. Mallot[e], C. Mariotti[ℓ,11], G. van Middelkoop[h], A. Milsztajn[i], Y. Mizuno[c,12], A. Most[c,13], A. Mücklich[c], J. Nassalski[n], D. Nowotny[c], J. Oberski[h], A. Paić[g], C. Peroni[ℓ], B. Povh[c,d], K. Prytz[m,14], R. Rieger[e], K. Rith[c,15], K. Röhrich[e,16], E. Rondio[n,2], L. Ropelewski[o,2], A. Sandacz[n], D. Sanders[17], C. Scholz[c], R. Seitz[e,18], F. Sever[a,h,19], T.-A. Shibata[d,20], M. Siebler[a], A. Simon[c,21], A. Staiano[ℓ], M. Szleper[n], W. Tłaczała[n,22], Y. Tzamouranis[c,17], M. Virchaux[i], J.L. Vuilleumier[g], T. Walcher[e], R. Windmolders[f], A. Witzmann[b], K. Zaremba[n,22], F. Zetsche[c,23]

[a] *Bielefeld University, Bielefeld, Germany*[24]
[b] *Freiburg University, Freiburg, Germany*[24]
[c] *Max-Planck Institut für Kernphysik, Heidelberg, Germany*[24]
[d] *Heidelberg University, Heidelberg, Germany*[24]
[e] *Mainz University, Mainz, Germany*[24]
[f] *Mons University, Mons, Belgium*
[g] *Neuchâtel University, Neuchâtel, Switzerland*
[h] *NIKHEF, Amsterdam, The Netherlands*[25]
[i] *Saclay DAPNIA/SPP, Saclay, France*[27]
[j] *University of California, Santa Cruz, USA*
[k] *Paul Scherrer Institut, Villigen, Switzerland*


*PII* S0550-3213(96)00537-8

[ℓ] Torino University and INFN Torino, Turin, Italy
[m] Uppsala University, Uppsala, Sweden
[n] Soltan Institute for Nuclear Studies, Warsaw, Poland[26]
[o] Warsaw University, Warsaw, Poland[26]

Received 3 September 1996; accepted 23 September 1996

**Abstract**

The $Q^2$ dependence of the structure function ratio $F_2^{Sn}/F_2^C$ for $0.01 < x < 0.75$ and $1 < Q^2 < 140$ GeV$^2$ is reported. For $x < 0.1$ the size of shadowing decreases linearly with $\ln Q^2$ and the maximum rate is about 0.04 at $x = 0.01$. The rate decreases with $x$ and is compatible with zero for $x \geqslant 0.1$. The difference $R^{Sn} - R^C$, where $R$ is the ratio of longitudinally to transversely polarised virtual photon absorption cross sections, is also given. No dependence on $x$ is seen and the average value is $0.040 \pm 0.021$ (stat.) $\pm 0.026$ (syst.) at a mean $Q^2$ of 10 GeV$^2$.

## 1. Introduction

It is well known that the structure function $F_2$ for a bound nucleon, measured in deep inelastic scattering (DIS) of leptons, differs from that for a free nucleon [1–6]. The

[1] Alexander von Humboldt fellow.
[2] Now at CERN, 1211 Geneva 23, Switzerland.
[3] Now at NIKHEF, 1009 DB Amsterdam, The Netherlands.
[4] Now at University of Padova, 35131 Padova, Italy.
[5] Now at MPI für Kernphysik, 69029 Heidelberg, Germany.
[6] Now at Université de Genève, 1211 Genève 4, Switzerland.
[7] Now at DPTA, CEA, Bruyères-le-Chatel, France.
[8] Now at Yale University, New Haven, 06511 CT, USA.
[9] Now at University of Mainz, 55099 Mainz, Germany.
[10] Now at University of Bonn, 53115 Bonn, Germany.
[11] Now at INFN-Istituto Superiore di Sanità, 00161 Roma, Italy.
[12] Now at Osaka University, 567 Osaka, Japan.
[13] Now at University of Michigan, Michigan, USA.
[14] Now at Stockholm University, 113 85 Stockholm, Sweden.
[15] Now at University of Erlangen-Nürnburg, 91058 Erlangen, Germany.
[16] Now at IKP2-KFA, 52428 Jülich, Germany.
[17] Now at University of Houston, 77204 TX, USA.
[18] Now at Dresden University, 01062 Dresden, Germany.
[19] Now at ESRF, 38043 Grenoble, France.
[20] Now at Tokyo Institute of Technology, Japan.
[21] Now at University of Freiburg, 79104 Freiburg, Germany.
[22] Now at Warsaw University of Technology, Warsaw, Poland.
[23] Now at DESY, 22603 Hamburg, Germany.
[24] Supported by Bundesministerium für Bildung und Forschung.
[25] Supported in part by FOM, Vrije Universiteit Amsterdam and NWO.
[26] Supported by KBN SPUB Nr 621/E - 78/SPUB/P3/209/94.
[27] Laboratory of CEA, Direction des Sciences de la Matière.

effect is usually presented in terms of the ratio $F_2^A/F_2^D$, where $F_2^A$ and $F_2^D$ are structure functions per nucleon of nucleus $A$ and the deuteron, respectively. Since the nucleons in the deuteron are only weakly bound, $F_2^D$ is taken to be a good approximation for the structure function of a free nucleon.

The dependence of $F_2^A/F_2^D$ on the atomic mass $A$ and on the Bjorken scaling variable $x$ has a characteristic pattern. For values of $x \lesssim 0.05$, the ratio is smaller than unity ("shadowing"). In the intermediate $x$ region, $0.05 \lesssim x \lesssim 0.2$, the ratio shows a small enhancement over unity. For larger values of $x$, up to about 0.6, the ratio decreases with increasing $x$. The size of all these effects grows with the atomic mass number $A$.

While the $A$ and $x$ dependences of $F_2^A/F_2^D$ are rather sizeable, with the ratio differing from unity by up to 30–40% for large $A$, so far no significant dependence on the photon virtuality $Q^2$ has been observed. The experimental results on the $Q^2$ dependence of $F_2^A/F_2^D$ are often presented in terms of the logarithmic slopes $\mathrm{d}(F_2^A/F_2^D)/\mathrm{d}(\ln Q^2)$. These slopes have been found to be typically less than 0.05 (for $Q^2$ expressed in $\mathrm{GeV}^2$) and consistent with zero [1–5].

The observed results can be described in the framework of different models [1]. For $x \gtrsim 0.1$, modifications of the nucleon characteristics inside a nucleus have been invoked; among them a reduced effective nucleon mass or an increase of the nucleon size. In the small $x$ region, attempts have been made to describe shadowing in terms of generalised vector meson dominance or of parton–parton fusion. A small decrease of shadowing with increasing $Q^2$ is expected in both approaches; the size of the effect is however smaller than the sensitivity of the measurements carried out so far.

In this paper we present the first observation of a $Q^2$ dependence for the ratio of nuclear structure functions. The data were collected using the NMC spectrometer at CERN with incident muon energies of 120, 200 and 280 GeV and cover the range $0.01 < x < 0.75$ and $1 < Q^2 < 140\ \mathrm{GeV}^2$. The $x$ dependence of the 200 GeV data was published in Ref. [6]. As discussed there, the choice of carbon as a reference nucleus instead of the deuteron was motivated by the requirement of large target thicknesses.

We also present the results for the difference $\Delta R = R^{Sn} - R^C$ of the ratios $R = \sigma_L/\sigma_T$ for Sn and C; here $\sigma_L$ and $\sigma_T$ are the cross sections for absorption of longitudinally and transversely polarised virtual photons, respectively. This difference $\Delta R$ was obtained by comparing the results found in given $x$ and $Q^2$ bins at different incident energies and thus different average virtual photon polarisations. Similar measurements were carried out at SLAC [7] for $R^{Fe} - R^D$ and $R^{Au} - R^D$ in the range $0.2 < x < 0.5$ and $1 < Q^2 < 5\ \mathrm{GeV}^2$ and by NMC [8] at CERN for $R^{Ca} - R^C$ in the range $0.007 < x < 0.2$ and $1 < Q^2 < 20\ \mathrm{GeV}^2$. The results of these experiments are consistent with no variation of $R$ with $A$. Only in this case can the structure function ratio $F_2^{A_1}/F_2^{A_2}$ be taken to be equal to the corresponding cross section ratio $\sigma^{A_1}/\sigma^{A_2}$; this assumption will be made throughout this paper. A dependence of $R$ on $A$ at small $x$ could indicate nuclear effects in the gluon distribution, or different higher twist contributions to $R^{A_1}$ and $R^{A_2}$.

In deep inelastic muon scattering from a nucleon, the double differential cross section per nucleon for one-photon exchange is given by

$$\frac{d^2\sigma_{l\gamma}}{dx\,dQ^2} = \frac{4\pi\alpha^2}{Q^4}\frac{F_2(x,Q^2)}{x}\left[1 - y - \frac{Q^2}{4E^2} + \left(1 - \frac{2m_\mu^2}{Q^2}\right)\frac{y^2 + Q^2/E^2}{2[1 + R(x,Q^2)]}\right], \quad (1)$$

where $F_2(x,Q^2)$ is the structure function of the nucleon and $R(x,Q^2) = \sigma_L/\sigma_T$. The variable $-Q^2$ is the four-momentum of the virtual photon squared, $E$ the incident muon energy, $\alpha$ the electromagnetic coupling constant and $m_\mu$ the muon mass. The Bjorken scaling variable $x$, and $y$ are defined as $x = Q^2/2M\nu$ and $y = \nu/E$, where $\nu$ is the energy of the virtual photon in the laboratory frame and $M$ the proton mass. The virtual photon–proton centre of mass energy will be indicated as $W$.

The paper is organised as follows. In Section 2 the features of the experiment relevant to the present analysis are described, in Section 3 the analysis is discussed and the results are presented in Section 4.

## 2. The experimental set-up

The experiment was performed with the NMC spectrometer at the CERN SPS muon beam line M2. Data were taken at incident muon energies of 120, 200 and 280 GeV. A detailed description of the spectrometer can be found in Ref. [9]. In the following we only give a brief overview of the target set-up and of the trigger conditions.

To perform accurate measurements of cross section ratios, a complementary target set-up was used; similar set-ups were employed in other NMC experiments. Two target sets were used, an upstream and a downstream one (cf. Fig. 1 of Ref. [6]). Each set consisted of two pairs of targets. A pair contained a target of tin and one of carbon, simultaneously exposed to the beam, one behind the other along the beam direction. The row of four targets simultaneously exposed to the beam was exchanged every 40 minutes with a complementary one, where the tin targets and the carbon ones were interchanged. The targets in a row were exposed to the same beam flux. Furthermore, the geometrical detector acceptance for events with a vertex at a given position along the beam was independent of the target material. The cross section ratio, $\sigma^{Sn}/\sigma^{C}$, for tin and carbon can then be expressed in a way that depends only on the number of reconstructed events, $N$, and on the number of nucleons per unit area, $T$, in the target [9]:

$$\left(\frac{\sigma^{Sn}}{\sigma^{C}}\right)_{meas} = \sqrt{\left(\frac{N^{Sn}_{Row1}N^{Sn}_{Row2}}{N^{C}_{Row1}N^{C}_{Row2}}\right)\left(\frac{T^{C}_{Row1}T^{C}_{Row2}}{T^{Sn}_{Row1}T^{Sn}_{Row2}}\right)}. \quad (2)$$

In this way the geometrical acceptance and detector efficiencies cancel, as do the beam fluxes. The formula was applied separately to the upstream and downstream target sets. The frequent exchange of the target rows substantially reduced the effects of possible time dependence of the acceptance and efficiency of the apparatus. The targets had a similar number of nucleons/cm$^2$, providing optimal statistical accuracy for the cross section ratio measurement. The carbon targets consisted of 75 cm long cylinders; the tin

ones of several equally spaced slices distributed over a length of 75 cm. The diameter of the targets was 7.5 cm. All targets were of natural isotopic composition.

The total target thickness exposed to the beam was about 600 g/cm$^2$. In order to shield the spectrometer from electromagnetic and hadronic background originating in such an amount of material, a calorimetric set-up was used [10,6] consisting of an iron-scintillator trigger calorimeter, a concrete-scintillator trigger calorimeter and a passive concrete absorber. The iron calorimeter was located between the upstream and downstream target sets; the concrete calorimeter was installed downstream of the targets. This arrangement made it possible to detect all hadronic showers emerging with angles of up to 20° with respect to the beam direction. In this way, for all events in which a scattered muon was seen by the NMC spectrometer, the accompanying hadrons were also measured. The passive absorber was designed to contain showers from the calorimeters; it consisted of five massive concrete blocks, separated by scintillator planes. The choice of materials and the shape of the calorimeters and of the absorber were such as to minimise the multiple scattering of the outgoing muon.

The iron and concrete calorimeters tagged deep inelastic interactions by the detection of the hadronic shower. The energy resolution for pions was about 25% at 10 GeV and 16% at 100 GeV. The calorimeter information was used only at the trigger level.

An energy deposit in the calorimeter above a given threshold was required for an event to be triggered. Muon interactions in the absorber did not release energy in the calorimeters and were therefore suppressed. A threshold corresponding to an energy release of 4 GeV for a hadronic shower gave a trigger efficiency close to 100%. In addition to the requirement of an energy deposit in the calorimeter, the standard "T1" trigger conditions described in Ref. [9] were applied, essentially demanding that a scattered muon be detected. The trigger was sensitive to muons scattered by more than $\approx 1°$ with respect to the incoming beam direction. A more restrictive angle cut of $\approx 2°$ was applied for the so-called "T2" trigger. The T1 trigger was prescaled to reduce the data acquisition dead time.

## 3. Analysis

Various kinematic cuts were applied to the data; they are summarised in Table 1. Events from regions with rapidly changing acceptance (small scattering angle $\vartheta$) and poor resolution (small $\nu$) were removed. The requirement $y < 0.85$ excluded kinematic regions where radiative corrections are large. A lower limit on the scattered muon momentum $p'$ was imposed, thereby rejecting muons originating from hadron decays. Events with poor vertex resolution due to multiple scattering, which is proportional to $1/(p'\vartheta)$, were suppressed by applying the cut $x > 0.01$, which corresponds to $p'\vartheta \gtrsim 1000$ GeV·mrad. The number of remaining events is $8.4 \times 10^6$. These data cover the kinematic region $0.01 < x < 0.75$ and $1 < Q^2 < 140$ GeV$^2$.

The data were corrected on an event by event basis for the trigger efficiency of the target calorimeter, which was parametrised as a function of $W^2$ for each individual

Table 1
Kinematic cuts applied to the data

| Muon energy | 120 GeV | 200 GeV | 280 GeV |
|---|---|---|---|
| $\nu$ [GeV] | > 10 | > 15 | > 20 |
| $p'$ [GeV] | > 20 | > 28 | > 40 |
| $W^2$ [GeV$^2$] | | > 20 | |
| $y$ | | < 0.85 | |
| $x$ | | > 0.01 | |
| $\vartheta$ [mrad] | | > 11 (upstream targets) | |
| | | > 13 (downstream targets) | |

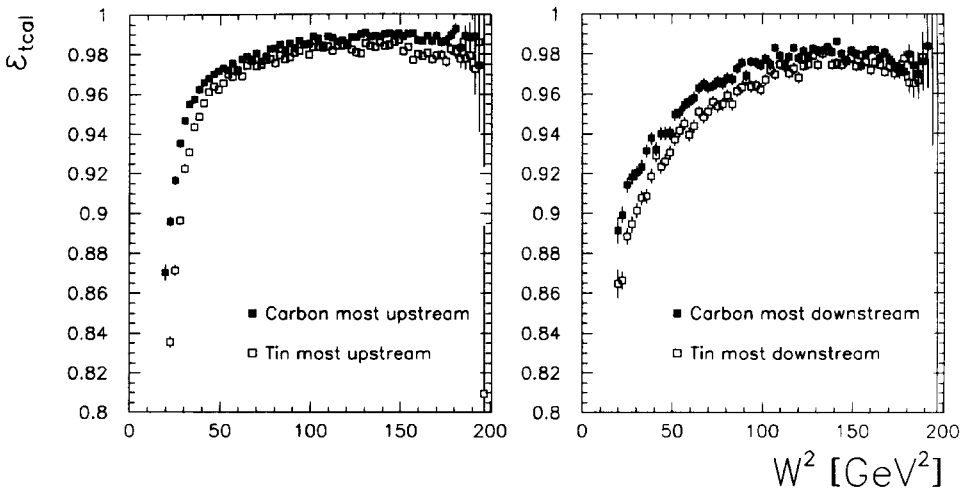


Fig. 1. Trigger efficiency of the target calorimeter as a function of $W^2$ for the most upstream (left) and the most downstream (right) *Sn* and *C* targets.

target. This efficiency was evaluated by using a sample of data in which the calorimeter was not demanded in the trigger. As an example, Fig. 1 shows the target calorimeter efficiency as a function of $W^2$ for Sn and C separately and for the most upstream and downstream target sets. For $W^2 > 20$ GeV$^2$, the efficiency is larger than 85%. The difference of a few per cent between the two targets is due to a different absorption of hadronic showers in the two target materials.

In order to obtain the one-photon exchange cross section ratio $(\sigma^{Sn}/\sigma^{C})_{1\gamma}$ from the measured cross section ratio (Eq. (2)), the measured yields were corrected for higher-order electroweak processes, notably for the radiative tails of coherent scattering from nuclei and quasielastic scattering from nucleons, as well as for the inelastic radiative tail. The threshold of the target calorimeter was equivalent to the energy release of 40–45 minimum ionising particles, which corresponded to 4 GeV for hadronic showers, as mentioned earlier, and to a somewhat lower energy for electromagnetic showers. For coherent and quasielastic events, the $\nu$ cuts applied (cf. Table 1) require a minimum

energy of the radiated photon of several GeV. This means that also these events satisfied the trigger, thereby requiring the application of the full coherent and quasielastic radiative corrections.

Each event was weighted with the correction factor $\eta = \sigma_{1\gamma}/\sigma_{\text{meas}}$, which was computed according to the scheme of Akhundov et al. [11]. Multiphoton exchange processes in the coherent radiative tail were also taken into account [12]; they amounted to less than 2% of the total radiative correction in the small $x$ region for tin and were negligible for carbon.

The calculation of the quasielastic radiative tails requires a parametrisation of the nucleon form factor which was taken from Ref. [13]. The quasielastic suppression factor, which takes into account the reduction of the elastic cross section for a bound nucleon with respect to a free one, was evaluated using the results of Bernabeu [14] for carbon and of Whitney et al. [15] for tin. For the evaluation of the coherent radiative tails, the nuclear elastic form factors are needed. A sum of Gaussians parametrisation was used for carbon [16] and a three-parameter Gaussian model was taken for tin [17].

Finally, in order to determine the inelastic tail contribution, the knowledge of $R(x,Q^2)$ and $F_2^{\text{A}}(x,Q^2)$ is needed. The ratio $R(x,Q^2)$ was taken from the SLAC parametrisation [18] and was assumed to be independent of the atomic mass $A$. The structure functions $F_2^{\text{C}}(x,Q^2)$ and $F_2^{\text{Sn}}(x,Q^2)$ were obtained using a parametrisation of $F_2^{\text{D}}$ [23], the ratio $F_2^{\text{C}}/F_2^{\text{D}}$ [4] and the ratio $F_2^{\text{Sn}}/F_2^{\text{C}}$:

$$F_2^{\text{C}}(x,Q^2) = F_2^{\text{D}}(x,Q^2)\frac{F_2^{\text{C}}}{F_2^{\text{D}}}(x), \tag{3}$$

$$F_2^{\text{Sn}}(x,Q^2) = F_2^{\text{C}}(x,Q^2)\frac{F_2^{\text{Sn}}}{F_2^{\text{C}}}(x,Q^2), \tag{4}$$

where the structure function ratio $F_2^{\text{C}}/F_2^{\text{D}}$ [4] was assumed to be independent of $Q^2$. For the ratio $F_2^{\text{Sn}}/F_2^{\text{C}}$, the presently measured cross section ratios as well as those on $F_2^{\text{Ag}}/F_2^{\text{C}}$ from the SLAC E139 experiment [2] were used. Since the measured ratio is needed as an input, an iterative procedure was used in the calculation of the radiative corrections.

The radiative correction factors, $\eta$, for the individual targets may vary over a wide range; in the case of tin from $\eta \approx 0.3$ at small $x$ to $\approx 1.1$ at large $x$. The dominant contribution to $\eta$ comes from the coherent radiative tail. For the ratio $F_2^{\text{Sn}}/F_2^{\text{C}}$ the resulting largest total correction is 0.4 in the lowest $x$ bin. The size of the correction decreases rapidly with increasing $x$ and differs from unity by less than 0.01 for $x > 0.05$.

The data were also corrected for the non-isoscalarity of the targets using a parametrisation of the structure function ratio $F_2^n/F_2^p$ [9]. This correction is maximum at large $x$ where it is at most 10%; it is negligible at small $x$.

As discussed in Ref. [6], the finite resolution of the spectrometer leads to an uncertainty in the position of the interaction vertex and in the determination of the kinematic variables. The dominant source of this smearing is multiple scattering of the muon which strongly affects events with small $p'\vartheta$ (small $x$). The effect of this on the cross section

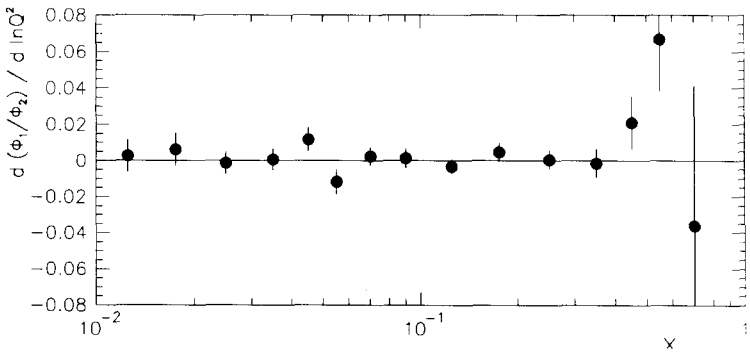


Fig. 2. The slopes $d(\Phi_1/\Phi_2)/d(\ln Q^2)$ from a linear fit in $\ln Q^2$ to the beam flux ratios for the two target rows, in bins of $x$. Errors shown are statistical only.

ratio was estimated by a Monte Carlo simulation. A description of the latter is given in Refs. [6,24,25].

The Monte Carlo was used to determine an $x$ and $Q^2$ dependent correction factor for the cross section ratio. For $x > 0.025$ the correction is less than 1% and increases to about 7% in the lowest $x$ bin.

As a check of the method to calculate the cross section ratio, following the reasoning presented in Ref. [9], the ratio of the beam fluxes for the two target rows was evaluated from the measured number of events. After applying all corrections, the flux ratio was studied as a function of all measured kinematic variables and found to be independent of them in the range where the results are presented. As an example, Fig. 2 shows the slopes $d(\Phi_1/\Phi_2)/d(\ln Q^2)$ from the linear fit in $\ln Q^2$ to the beam flux ratio $\Phi_1/\Phi_2$ for the two target rows, in bins of $x$.

## 4. The results

### 4.1. $x$ and $Q^2$ dependence

The $x$ dependence of the structure function ratio $F_2^{Sn}/F_2^C$, averaged over $Q^2$, is presented in Fig. 3 and in Table 2. It was obtained after combining the data taken at the three different energies. The mean $Q^2$ and mean $y$ for each $x$ bin is also given in the table. The inner error bars in Fig. 3 represent the statistical uncertainties – including that of the smearing correction factor. The outer error bars indicate the size of the statistical and systematic uncertainties added in quadrature. The figure also shows the E139 results for $F_2^{Ag}/F_2^C$, obtained from Ref. [2] by dividing the published ratios $F_2^{Ag}/F_2^D$ and $F_2^C/F_2^D$. To calculate the ratio $F_2^{Ag}/F_2^C$ the errors were treated as uncorrelated and no correction for a possible $Q^2$ dependence was applied. The present result confirms the well known $x$ dependence of nuclear effects in the structure function $F_2$.

The ratio $F_2^{Sn}/F_2^C$ in bins of $x$ and $Q^2$ is given in Table 3. Fig. 4 shows the ratios as a function of $Q^2$ in each $x$ bin. The lines indicate the results of fits of the

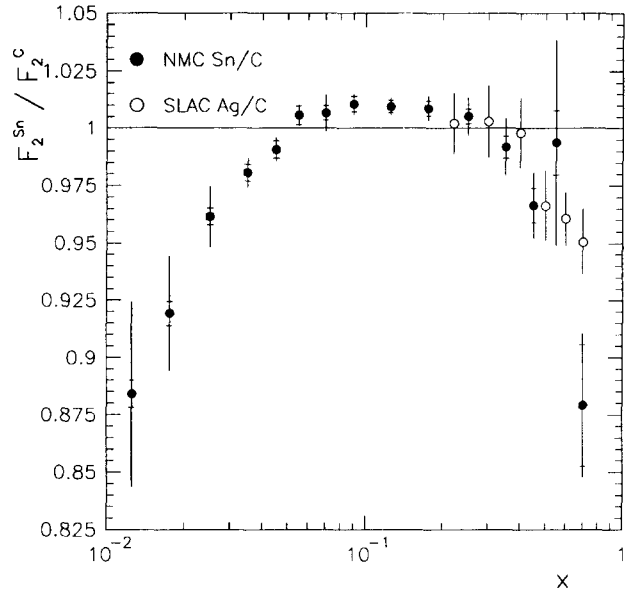


Fig. 3. Structure function ratios as a function of $x$, averaged over $Q^2$. The inner error bars represent the statistical uncertainty, the outer errors the statistical and systematic uncertainties added in quadrature. The normalisation error is 0.2% and is not included in the systematic uncertainty. The SLAC-E139 [2] ratios for silver and carbon are also plotted (open points).

Table 2
The ratio $F_2^{Sn}/F_2^{C}$ as a function of $x$. The $x$ value, the mean $Q^2$ and the mean $y$ are also given. The normalisation error on the ratio is 0.2% and is not included in the systematic uncertainty

| $x$ | $\langle Q^2 \rangle$ [GeV$^2$] | $\langle y \rangle$ | $F_2^{Sn}/F_2^{C} \pm$ stat. $\pm$ syst. |
|---|---|---|---|
| 0.0125 | 3.3 | 0.72 | 0.884±0.006±0.040 |
| 0.0175 | 4.3 | 0.67 | 0.919±0.005±0.025 |
| 0.025 | 5.6 | 0.61 | 0.961±0.004±0.013 |
| 0.035 | 7.2 | 0.54 | 0.981±0.004±0.007 |
| 0.045 | 8.6 | 0.48 | 0.991±0.004±0.005 |
| 0.055 | 9.9 | 0.43 | 1.006±0.004±0.005 |
| 0.070 | 11.4 | 0.37 | 1.007±0.003±0.008 |
| 0.090 | 13.1 | 0.31 | 1.011±0.004±0.005 |
| 0.125 | 15.2 | 0.25 | 1.009±0.003±0.004 |
| 0.175 | 17.9 | 0.21 | 1.009±0.004±0.005 |
| 0.25 | 20.8 | 0.18 | 1.005±0.003±0.008 |
| 0.35 | 26.6 | 0.16 | 0.992±0.005±0.013 |
| 0.45 | 35.1 | 0.17 | 0.966±0.008±0.014 |
| 0.55 | 44.8 | 0.18 | 0.994±0.015±0.045 |
| 0.70 | 65.8 | 0.22 | 0.88±0.03±0.03 |

function $F_2^{Sn}/F_2^{C} = a + b \ln Q^2$ in each bin. Fig. 5 shows the logarithmic slopes $b$ as a function of $x$. The slopes are positive and significantly different from zero in the region $0.01 < x < 0.05$, indicating that the amount of shadowing decreases with increasing $Q^2$.

Table 3
The ratio $F_2^{Sn}/F_2^C$ as a function of $x$ and $Q^2$. The $x$ value and the mean $Q^2$ are also given. The normalisation error on the ratio is 0.2% and is not included in the systematic uncertainty

| $x$ | $Q^2$ [GeV$^2$] | $F_2^{Sn}/F_2^C \pm$ stat. $\pm$ syst. |
|---|---|---|
| 0.0125 | 1.3 | 0.858 ± 0.017 ± 0.022 |
| 0.0125 | 1.8 | 0.876 ± 0.014 ± 0.034 |
| 0.0125 | 2.3 | 0.839 ± 0.019 ± 0.035 |
| 0.0125 | 2.8 | 0.881 ± 0.019 ± 0.035 |
| 0.0125 | 3.5 | 0.890 ± 0.015 ± 0.042 |
| 0.0125 | 4.5 | 0.902 ± 0.013 ± 0.048 |
| 0.0125 | 5.5 | 0.925 ± 0.019 ± 0.056 |
| 0.0125 | 7.0 | 0.93 ± 0.06 ± 0.07 |
| 0.0175 | 1.3 | 0.83 ± 0.03 ± 0.10 |
| 0.0175 | 1.8 | 0.880 ± 0.016 ± 0.023 |
| 0.0175 | 2.3 | 0.895 ± 0.015 ± 0.018 |
| 0.0175 | 2.8 | 0.920 ± 0.017 ± 0.026 |
| 0.0175 | 3.5 | 0.945 ± 0.014 ± 0.027 |
| 0.0175 | 4.5 | 0.931 ± 0.014 ± 0.028 |
| 0.0175 | 5.5 | 0.920 ± 0.013 ± 0.033 |
| 0.0175 | 7.0 | 0.939 ± 0.012 ± 0.037 |
| 0.0175 | 9.0 | 0.97 ± 0.05 ± 0.06 |
| 0.025 | 1.8 | 0.937 ± 0.018 ± 0.027 |
| 0.025 | 2.3 | 0.929 ± 0.013 ± 0.020 |
| 0.025 | 2.8 | 0.944 ± 0.013 ± 0.013 |
| 0.025 | 3.5 | 0.961 ± 0.009 ± 0.013 |
| 0.025 | 4.5 | 0.949 ± 0.010 ± 0.013 |
| 0.025 | 5.5 | 0.961 ± 0.012 ± 0.014 |
| 0.025 | 7.0 | 0.973 ± 0.008 ± 0.015 |
| 0.025 | 9.0 | 0.981 ± 0.010 ± 0.021 |
| 0.025 | 11.5 | 0.981 ± 0.016 ± 0.031 |
| 0.035 | 1.8 | 0.98 ± 0.03 ± 0.03 |
| 0.035 | 2.3 | 0.95 ± 0.02 ± 0.03 |
| 0.035 | 2.8 | 0.963 ± 0.017 ± 0.010 |
| 0.035 | 3.5 | 0.972 ± 0.011 ± 0.006 |
| 0.035 | 4.5 | 0.971 ± 0.011 ± 0.009 |
| 0.035 | 5.5 | 0.963 ± 0.011 ± 0.013 |
| 0.035 | 7.0 | 0.980 ± 0.009 ± 0.006 |
| 0.035 | 9.0 | 0.996 ± 0.009 ± 0.015 |
| 0.035 | 11.5 | 0.996 ± 0.009 ± 0.011 |
| 0.035 | 15.0 | 0.993 ± 0.014 ± 0.016 |
| 0.035 | 20.0 | 0.92 ± 0.10 ± 0.07 |
| 0.045 | 1.8 | 0.96 ± 0.04 ± 0.13 |
| 0.045 | 2.3 | 0.97 ± 0.03 ± 0.03 |
| 0.045 | 2.8 | 0.981 ± 0.022 ± 0.019 |
| 0.045 | 3.5 | 0.973 ± 0.014 ± 0.022 |
| 0.045 | 4.5 | 1.000 ± 0.013 ± 0.016 |
| 0.045 | 5.5 | 0.979 ± 0.012 ± 0.004 |
| 0.045 | 7.0 | 0.971 ± 0.009 ± 0.016 |
| 0.045 | 9.0 | 1.010 ± 0.011 ± 0.019 |
| 0.045 | 11.5 | 1.002 ± 0.009 ± 0.006 |
| 0.045 | 15.0 | 0.993 ± 0.010 ± 0.006 |
| 0.045 | 20.0 | 1.010 ± 0.018 ± 0.013 |

Table 3 — continued

| $x$ | $Q^2$ [GeV$^2$] | $F_2^{Sn}/F_2^C \pm$ stat. $\pm$ syst. |
|---|---|---|
| 0.055 | 2.3 | 0.97 ± 0.03 ± 0.04 |
| 0.055 | 2.8 | 0.93 ± 0.03 ± 0.04 |
| 0.055 | 3.5 | 1.018 ± 0.017 ± 0.008 |
| 0.055 | 4.5 | 1.015 ± 0.016 ± 0.028 |
| 0.055 | 5.5 | 1.006 ± 0.015 ± 0.007 |
| 0.055 | 7.0 | 0.996 ± 0.010 ± 0.022 |
| 0.055 | 9.0 | 1.014 ± 0.011 ± 0.013 |
| 0.055 | 11.5 | 1.008 ± 0.010 ± 0.004 |
| 0.055 | 15.0 | 1.008 ± 0.010 ± 0.004 |
| 0.055 | 20.0 | 1.015 ± 0.012 ± 0.007 |
| 0.055 | 27.0 | 0.98 ± 0.03 ± 0.02 |
| 0.070 | 2.3 | 0.93 ± 0.03 ± 0.06 |
| 0.070 | 2.8 | 0.99 ± 0.02 ± 0.03 |
| 0.070 | 3.5 | 1.013 ± 0.015 ± 0.011 |
| 0.070 | 4.5 | 1.020 ± 0.014 ± 0.009 |
| 0.070 | 5.5 | 0.992 ± 0.013 ± 0.010 |
| 0.070 | 7.0 | 0.993 ± 0.009 ± 0.006 |
| 0.070 | 9.0 | 1.013 ± 0.009 ± 0.016 |
| 0.070 | 11.5 | 1.010 ± 0.008 ± 0.007 |
| 0.070 | 15.0 | 1.010 ± 0.008 ± 0.004 |
| 0.070 | 20.0 | 1.006 ± 0.008 ± 0.012 |
| 0.070 | 27.0 | 1.028 ± 0.012 ± 0.005 |
| 0.070 | 36.0 | 0.94 ± 0.04 ± 0.03 |
| 0.090 | 2.3 | 0.99 ± 0.04 ± 0.06 |
| 0.090 | 2.8 | 0.99 ± 0.03 ± 0.05 |
| 0.090 | 3.5 | 1.00 ± 0.02 ± 0.02 |
| 0.090 | 4.5 | 0.99 ± 0.02 ± 0.04 |
| 0.090 | 5.5 | 1.007 ± 0.016 ± 0.013 |
| 0.090 | 7.0 | 1.013 ± 0.011 ± 0.015 |
| 0.090 | 9.0 | 1.025 ± 0.011 ± 0.014 |
| 0.090 | 11.5 | 1.011 ± 0.009 ± 0.008 |
| 0.090 | 15.0 | 1.011 ± 0.008 ± 0.003 |
| 0.090 | 20.0 | 1.021 ± 0.009 ± 0.007 |
| 0.090 | 27.0 | 0.999 ± 0.011 ± 0.006 |
| 0.090 | 36.0 | 1.000 ± 0.017 ± 0.012 |
| 0.125 | 2.3 | 0.80 ± 0.07 ± 0.11 |
| 0.125 | 2.8 | 0.98 ± 0.03 ± 0.04 |
| 0.125 | 3.5 | 0.997 ± 0.016 ± 0.011 |
| 0.125 | 4.5 | 1.003 ± 0.014 ± 0.024 |
| 0.125 | 5.5 | 1.028 ± 0.014 ± 0.020 |
| 0.125 | 7.0 | 0.998 ± 0.009 ± 0.007 |
| 0.125 | 9.0 | 1.000 ± 0.009 ± 0.005 |
| 0.125 | 11.5 | 1.012 ± 0.007 ± 0.003 |
| 0.125 | 15.0 | 1.016 ± 0.006 ± 0.006 |
| 0.125 | 20.0 | 1.008 ± 0.006 ± 0.014 |
| 0.125 | 27.0 | 1.020 ± 0.007 ± 0.003 |
| 0.125 | 36.0 | 1.006 ± 0.010 ± 0.016 |
| 0.125 | 48.0 | 1.013 ± 0.015 ± 0.010 |
| 0.125 | 65.0 | 1.03 ± 0.06 ± 0.08 |
| 0.175 | 3.5 | 0.96 ± 0.05 ± 0.03 |
| 0.175 | 4.5 | 0.96 ± 0.02 ± 0.04 |

Table 3 — continued

| $x$ | $Q^2$ [GeV$^2$] | $F_2^{Sn}/F_2^C \pm$ stat. $\pm$ syst. |
|---|---|---|
| 0.175 | 5.5 | 1.041 ± 0.020 ± 0.016 |
| 0.175 | 7.0 | 1.039 ± 0.013 ± 0.018 |
| 0.175 | 9.0 | 1.005 ± 0.012 ± 0.011 |
| 0.175 | 11.5 | 1.026 ± 0.010 ± 0.006 |
| 0.175 | 15.0 | 0.996 ± 0.008 ± 0.004 |
| 0.175 | 20.0 | 1.006 ± 0.008 ± 0.008 |
| 0.175 | 27.0 | 1.009 ± 0.009 ± 0.007 |
| 0.175 | 36.0 | 1.018 ± 0.011 ± 0.007 |
| 0.175 | 48.0 | 0.990 ± 0.014 ± 0.014 |
| 0.175 | 65.0 | 1.00 ± 0.02 ± 0.05 |
| 0.25 | 5.5 | 1.03 ± 0.04 ± 0.03 |
| 0.25 | 7.0 | 0.991 ± 0.015 ± 0.014 |
| 0.25 | 9.0 | 0.988 ± 0.012 ± 0.007 |
| 0.25 | 11.5 | 1.012 ± 0.010 ± 0.011 |
| 0.25 | 15.0 | 1.009 ± 0.008 ± 0.011 |
| 0.25 | 20.0 | 1.002 ± 0.007 ± 0.012 |
| 0.25 | 27.0 | 1.001 ± 0.008 ± 0.007 |
| 0.25 | 36.0 | 1.013 ± 0.010 ± 0.005 |
| 0.25 | 48.0 | 1.000 ± 0.011 ± 0.006 |
| 0.25 | 65.0 | 1.020 ± 0.016 ± 0.006 |
| 0.25 | 110.0 | 1.04 ± 0.03 ± 0.04 |
| 0.35 | 9.0 | 0.92 ± 0.04 ± 0.03 |
| 0.35 | 11.5 | 0.98 ± 0.02 ± 0.04 |
| 0.35 | 15.0 | 0.998 ± 0.013 ± 0.012 |
| 0.35 | 20.0 | 1.006 ± 0.010 ± 0.009 |
| 0.35 | 27.0 | 0.988 ± 0.011 ± 0.029 |
| 0.35 | 36.0 | 0.977 ± 0.013 ± 0.011 |
| 0.35 | 48.0 | 1.015 ± 0.016 ± 0.018 |
| 0.35 | 65.0 | 0.990 ± 0.018 ± 0.007 |
| 0.35 | 110.0 | 0.98 ± 0.02 ± 0.03 |
| 0.45 | 15.0 | 0.96 ± 0.03 ± 0.05 |
| 0.45 | 20.0 | 0.991 ± 0.015 ± 0.025 |
| 0.45 | 27.0 | 0.963 ± 0.015 ± 0.022 |
| 0.45 | 36.0 | 0.985 ± 0.018 ± 0.012 |
| 0.45 | 48.0 | 0.947 ± 0.021 ± 0.022 |
| 0.45 | 65.0 | 0.926 ± 0.025 ± 0.019 |
| 0.45 | 110.0 | 0.944 ± 0.028 ± 0.012 |
| 0.55 | 20.0 | 1.07 ± 0.06 ± 0.06 |
| 0.55 | 27.0 | 0.974 ± 0.024 ± 0.019 |
| 0.55 | 36.0 | 1.00 ± 0.03 ± 0.06 |
| 0.55 | 48.0 | 0.94 ± 0.04 ± 0.05 |
| 0.55 | 65.0 | 1.05 ± 0.04 ± 0.03 |
| 0.55 | 110.0 | 1.02 ± 0.04 ± 0.06 |
| 0.70 | 36.0 | 0.82 ± 0.06 ± 0.14 |
| 0.70 | 48.0 | 0.93 ± 0.05 ± 0.09 |
| 0.70 | 65.0 | 0.94 ± 0.05 ± 0.03 |
| 0.70 | 110.0 | 0.77 ± 0.06 ± 0.19 |

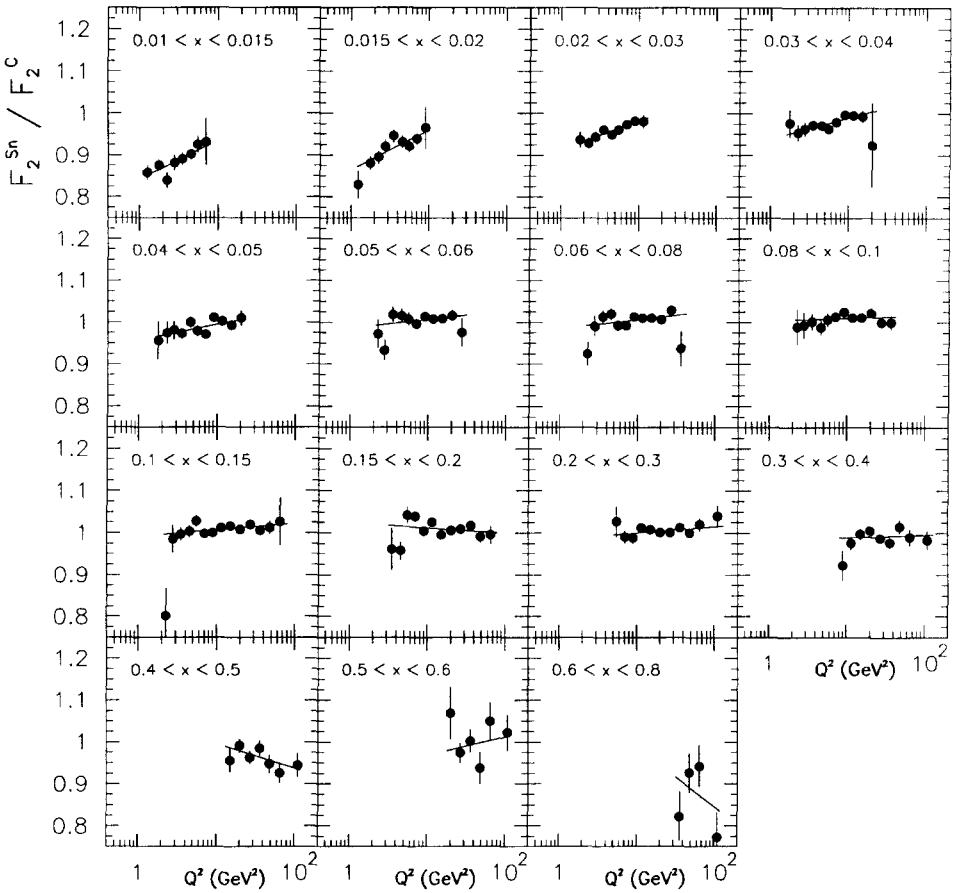


Fig. 4. Structure function ratios $F_2^{Sn}/F_2^C$ as a function of $Q^2$ in different $x$ bins. The error bars give the statistical uncertainty. The solid lines represent the result of fits of the function $F_2^{Sn}/F_2^C = a + b \ln Q^2$ in each $x$ bin.

Our results are consistent with those of previous measurements of the $Q^2$ dependence of $F_2^{A_1}/F_2^{A_2}$, which however had uncertainties larger than the size of the presently observed effect [1–5].

The main contributions to the systematic errors at small $x$ are the uncertainties in the radiative corrections. These uncertainties were estimated by varying the input parameters to the radiative correction program, following the procedure outlined in Ref. [9]. The inputs $F_2^D$ and $F_2^C/F_2^D$ were varied between their lower and upper limits, including statistical and systematic uncertainties, while for the function $R$ we used its systematic errors according to the parameterisation of Ref. [18]. An alternative parametrisation of the nucleon form factor was taken from Ref. [19]. The quasielastic suppression factor for carbon was recalculated using the results of Ref. [15], while for tin an uncertainty of 20% was assumed. Finally, for the nuclear elastic form factors, the Fourier transform of the charge distribution was used for carbon [20] and for tin a generalised two-parameter

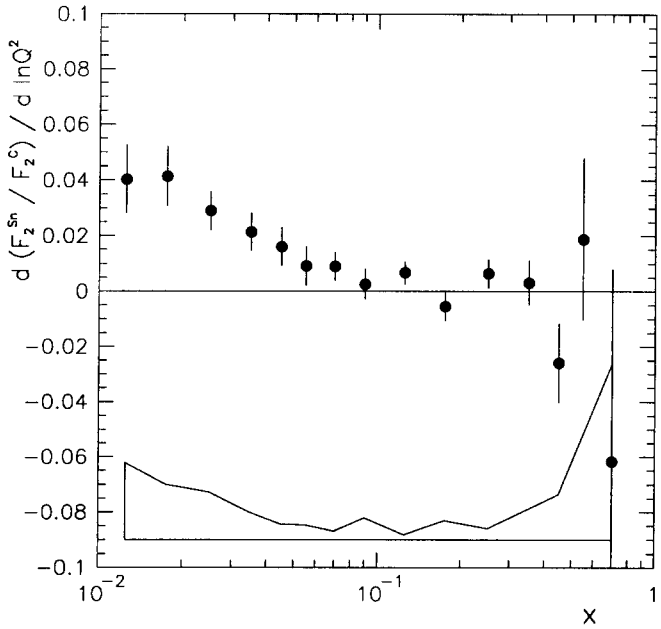


Fig. 5. The slopes $b$ from a linear fit in $\ln Q^2$ in each $x$ bin separately. The error bars represent the statistical uncertainty. The band shows the size of the systematic uncertainty.

Fermi charge distribution was adopted [21]. It was checked that tighter cuts on $y$ do not change the results. Altogether, the uncertainties due to the radiative corrections are about 4% on the ratio and 0.02 on its slope with respect to $\ln Q^2$ at the smallest value of $x$ and they decrease with increasing $x$.

Other contributions to the systematic error at small $x$ include the uncertainty of the smearing correction. This was estimated by changing the vertex resolution in the Monte Carlo by up to 3%, hence effectively modifying the amount of multiple Coulomb scattering. The corresponding variations of the ratio and of the slope were at most 1% and 0.005, respectively. As an estimate of the systematic uncertainty due to the target calorimeter efficiency determination, the latter was parametrised using different functional forms; the effect is maximum at large $x$, where it is less than 1% on the ratio and less than 0.02 on the $Q^2$ slope. The uncertainty on the measurement of incoming ($\delta p/p = 0.2\%$) and scattered muon momenta ($\delta p'/p' = 0.2\%$) and the uncertainty introduced by the isoscalarity correction were also taken into account. They are relevant only at large $x$ and are smaller than 1% for the ratio and 0.005 for the slope.

An additional systematic error of up to 1% on the ratio and 0.01 on the slope at small $x$ was included as an estimate of the uncertainty of the complementary target method used to extract the ratios. This was estimated by evaluating the $x$ and $Q^2$ dependences of the ratio with the following two methods:

(i) The upstream and the downstream target sets were treated separately, effectively leading to two independent determinations of the ratio in each $x$ and $Q^2$ bin.

(ii) A fit was used to extract the ratio, in which the cross section ratio, the beam flux ratio for the two target rows and the ratios of the geometric acceptances for different target positions were fitted simultaneously, as discussed in Ref. [6].

The difference between the results obtained with these two methods and the nominal one were summed in quadrature and taken as an estimate of the uncertainty of the complementary target method.

All contributions to the systematic uncertainty were summed in quadrature, apart from the normalisation uncertainty on the ratios due to the uncertainties in the target thicknesses which amounts to 0.2%. The normalisation uncertainty is not included in the errors given in the tables and shown in the figures.

Under the assumption that $dF_2^A/d\ln Q^2$ is similar for all nuclei, which is compatible with equal gluon distributions for Sn and C at small $x$, it is straightforward to show that

$$b = \frac{d(F_2^{Sn}/F_2^C)}{d\ln Q^2} = \left(1 - \frac{F_2^{Sn}}{F_2^C}\right)\frac{d\ln F_2^C}{d\ln Q^2}. \tag{5}$$

In the range $0.01 < x < 0.06$, the first factor in Eq. (5) is between 0.1 and 0, whereas $d\ln F_2^C/d\ln Q^2 = (F_2^D/F_2^C)\cdot d\ln F_2^D/d\ln Q^2$ is between 0.3 and 0.1 (see Refs. [4,22]). Hence one expects a logarithmic slope $b$ decreasing from about 0.03 at the smallest $x$ value to zero at $x \approx 0.06$. This is consistent with the observed effect.

Simple leading order perturbative QCD calculations, in which it is assumed that the $Q^2$ dependence in the structure function ratio arises solely from the difference in the $x$ dependence of the two structure functions, are also able to approximately account for the observed $Q^2$ dependence of $F_2^{Sn}/F_2^C$ [25].

### 4.2. $R^{Sn} - R^C$

To extract $\Delta R = R^{Sn} - R^C$ the method described in Ref. [8] was used. We briefly recall the main points here.

The function $R$ is sensitive to the differences in cross sections measured at different incident muon energies. For a given $(x, Q^2)$ bin the cross section ratio $\sigma^{Sn}/\sigma^C$ for an incident muon energy $E_i$ can be written as

$$\frac{\sigma^{Sn}}{\sigma^C}(E_i) = \frac{F_2^{Sn}}{F_2^C}\frac{1+R^C}{1+R^{Sn}}\frac{1+z_iR^{Sn}}{1+z_iR^C} \approx \frac{F_2^{Sn}}{F_2^C}\left[1 - \frac{1-z_i}{(1+\bar{R})(1+z_i\bar{R})}\Delta R\right], \tag{6}$$

where

$$z_i = \frac{1}{1+\frac{1}{2}(y_i^2 + Q^2/E_i^2)/(1-y_i-Q^2/4E_i^2)}, \tag{7}$$

with $y_i = \nu/E_i$ and $\bar{R} = \frac{1}{2}(R^{Sn} + R^C)$; the $z_i$ coefficients are always smaller than unity and mainly depend on $y_i$.

For each $x$ bin a parametrisation with the form of Eq. (6) was fitted simultaneously to the data at each incident muon energy for all values of $Q^2$. The parametrisation had four free parameters: the mean value of $\Delta R$ in the bin, and the three parameters $a_1$,

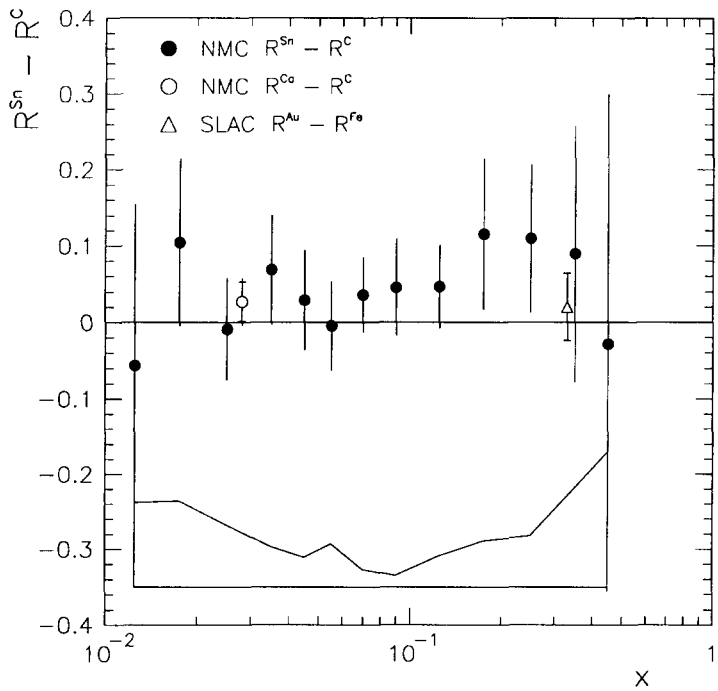


Fig. 6. The measured values of $R^{Sn} - R^{C}$ as a function of $x$. The error bars represent the statistical uncertainty. The band shows the size of the systematic uncertainty. Also shown are the NMC result for the average value of $R^{Ca} - R^{C}$ [8] (open circle) and the SLAC one for $R^{Au} - R^{Fe}$ [7] (triangle).

$a_2$ and $a_3$ of the function $F_2^{Sn}/F_2^{C} = (a_1 + a_2 \ln Q^2)(1 + a_3/Q^2)$ describing the $Q^2$ dependence of the structure function ratio in this $x$ bin. The quantity $\bar{R}$ was taken to be equal to the SLAC parametrisation [18] with artificially large errors. The dependence of $\Delta R$ on $\bar{R}$ is weak. The fits describe the data well in all $x$ bins, with a total $\chi^2$/d.o.f. of 276/325. It was checked that the coefficients $a_2$ were consistent with the values of $b$ found in the analysis of the $Q^2$ dependence and that the coefficients $a_3$ were compatible with zero.

The values of $\Delta R$ resulting from the fits are shown in Fig. 6 as a function of $x$ and listed in Table 4. They cover the range $0.01 < x < 0.5$. Also shown in Fig. 6 are the average values of the NMC measurement of $\Delta R = R^{Ca} - R^{C}$ [8] and of $\Delta R = R^{Au} - R^{Fe}$ deduced from the measurements of the E140 experiment at SLAC [7].

Since no significant $x$ dependence of $\Delta R$ was observed, we averaged the measurements over $x$ and obtained at a mean $Q^2$ of 10 GeV$^2$

$$\Delta R = R^{Sn} - R^{C} = 0.040 \pm 0.021 \text{ (stat.)} \pm 0.026 \text{ (syst.)}. \tag{8}$$

If the measured value of $\Delta R$ is assumed in the analysis of the $Q^2$ dependence of the structure function ratios, the logarithmic slopes $b$ change by at most 0.006.

Table 4
The measured values of $\Delta R = R^{Sn} - R^{C}$ as a function of $x$. Also given is the mean value of $Q^2$ in each $x$ bin

| $x$ | $\langle Q^2 \rangle$ [GeV$^2$] | $\Delta R \pm$ stat. $\pm$ syst. |
|---|---|---|
| 0.0125 | 3.3 | $-0.06 \pm 0.21 \pm 0.11$ |
| 0.0175 | 4.3 | $0.10 \pm 0.11 \pm 0.11$ |
| 0.025 | 5.6 | $-0.01 \pm 0.07 \pm 0.08$ |
| 0.035 | 7.2 | $0.07 \pm 0.07 \pm 0.05$ |
| 0.045 | 8.6 | $0.03 \pm 0.07 \pm 0.04$ |
| 0.055 | 9.9 | $0.00 \pm 0.06 \pm 0.06$ |
| 0.070 | 11.4 | $0.04 \pm 0.05 \pm 0.02$ |
| 0.090 | 13.1 | $0.05 \pm 0.06 \pm 0.02$ |
| 0.125 | 15.2 | $0.05 \pm 0.05 \pm 0.04$ |
| 0.175 | 17.9 | $0.12 \pm 0.10 \pm 0.06$ |
| 0.25 | 20.8 | $0.11 \pm 0.10 \pm 0.07$ |
| 0.35 | 26.6 | $0.09 \pm 0.17 \pm 0.13$ |
| 0.45 | 35.1 | $-0.03 \pm 0.33 \pm 0.18$ |

## References


[1] For a review see, e.g., T. Sloan, G. Smadja and R. Voss, Phys. Rep. 162 (1988) 45;
L. Frankfurt and M. Strikman, Phys. Rep. 160 (1988) 235;
R.J.M. Covolan, E. Predazzi, *in* Problems of Fundamental Modern Physics, ed. R. Cherubini, P. Dalpiaz and B. Minetti (World Scientific, Singapore, 1991) p. 85;
M. Arneodo, Phys. Rep. 240 (1994) 301.
[2] SLAC-E139, R.G. Arnold et al., Phys. Rev. Lett. 52 (1984) 727;
R.G. Arnold et al., SLAC Report SLAC-PUB-3257 (1983);
J. Gomez et al., Phys. Rev. D 49 (1994) 4348.
[3] NMC, M. Arneodo et al., Nucl. Phys. B 441 (1995) 3.
[4] NMC, M. Arneodo et al., Nucl. Phys. B 441 (1995) 12.
[5] FNAL E665, M.R. Adams et al., Z. Phys. C 67 (1995) 403.
[6] NMC, M. Arneodo et al., Nucl. Phys. B 481 (1996) 3, preceding article in this issue.
[7] SLAC E140, S. Dasu et al., Phys. Rev. Lett. 60 (1988) 2591.
[8] NMC, P. Amaudruz et al., Phys. Lett. B 294 (1992) 120.
[9] NMC, P. Amaudruz et al., Nucl. Phys. B 371 (1992) 3.
[10] F. Zetsche, Ph.D. thesis, Heidelberg University (1990), unpublished (in German).
[11] A.A. Akhundov et al., DESY 94-115(1994); CERN-TH 7339/94 (1994); IC/94/154 (1994); and to appear in Progress of Physics.
[12] K. Kurek, Z. Phys. C 63 (1994) 561.
[13] M. Gari and W. Krümpelmann, Z. Phys. A 322 (1985) 689.
[14] J. Bernabeu, Nucl. Phys. B 49 (1972) 186.
[15] R.J. Whitney et al., Phys. Rev. C 9 (1974) 2230.
[16] I. Sick, Phys. Lett. B 116 (1982) 212.
[17] J.R. Ficenec et al., Phys. Lett. B 42 (1972) 213.
[18] L.W. Whitlow et al., Phys. Lett. B 250 (1990) 193.
[19] W.B. Atwood, PhD thesis, Standford University (1972), SLAC-185, UC-34D (1975).
[20] I. Sick and J.S. McCarthy, Nucl. Phys. A 150 (1970) 63.
[21] A. Bohr and B. Mottelson, Nuclear Structure (Benjamin, New York, 1969).
[22] NMC, M. Arneodo et al., Phys. Lett. B 309 (1994) 222.
[23] NMC, P. Amaudruz et al., Phys. Lett. B 295 (1992) 159.
[24] A. Mücklich, PhD thesis, Heidelberg University (1995), unpublished (in German).
[25] M. Szleper, PhD thesis, Soltan Institute for Nuclear Studies, Warsaw (1995), unpublished.
[26] H. De Vries et al., Atomic Data and Nuclear Data Tables, 36 (1987) 495.